Effects of diglyme on Au nanocluster formation: Mechanism, ^{1}H NMR, and Bonding

Yuchen Wang,[1] Alice Li,[1,2] Jacqueline Pinkerton,[1,3] Christine M. Aikens[1,*]

1. Department of Chemistry, Kansas State University, Manhattan, KS 66506, USA
2. Department of Chemistry and Biochemistry, Bates College, Lewiston, ME 04240, USA
3. Natural Sciences Programs, Pensacola Christian College, Pensacola, FL 32503, USA

*Email: cmaikens@ksu.edu; Phone: 1-785-532-0954

Abstract

Recently, diglyme was applied as a solvent in the synthesis of a luminescent gold-thiolate nanocluster. However, the interactions between the diglyme and the gold nanocluster and the intrinsic mechanism of the diglyme-assisted nanocluster growth have not been examined. In this work, we use density functional theory (DFT) to propose a plausible pathway for diglyme-assisted Au(I)-thiolate synthesis; the reaction energies are found to be negative in every step. ^{1}H NMR calculations are applied to characterize how the environment arising from different gold motifs affects the chemical shifts of the protons on diglyme, which experience strong downfield shifts. Extended transition state - natural orbitals for chemical valence (ETS-NOCV) theory is also utilized to examine the interactions between diglyme and gold clusters as well as a $Au_{20}(SR)_{15}$ nanocluster. Our work demonstrates that diglyme can play an important role in the synthetic mechanism yielding gold nanoclusters and provides insights into the diglyme-nanocluster binding motifs and resulting NMR chemical shifts.

Introduction

Ligand-protected gold thiolate nanoclusters have shown several unique physical and chemical properties which can be applied to diverse areas such as photocatalysis,[1] biomedicine,[2] and chemical or biomedical sensors.[3] Most gold-thiolate nanoclusters are found to be "atomically precise nanoclusters",[4] such as $Au_{20}(SR)_{16}$,[5,6] $Au_{25}(SR)_{18}^-$,[7–9] $Au_{38}(SR)_{24}$,[10,11] and $Au_{104}(SR)_{46}$.[12] The general structure of a gold-thiolate nanocluster consists of a gold kernel and gold-thiolate protecting motifs (of which the basic unit is SR-Au-SR).[13] The R group on the thiolate (SR) ligand

can be SPh, SCH_2CH_2Ph (aka PET, phenylethanethiolate), *p*-MBA (*para*-mercaptobenzoic acid), etc.

The Brust–Schiffrin (B-S) method was one of the earliest methods to synthesize gold-thiolate nanoclusters. The B-S method starts with a Au(III) complex (such as $HAuCl_4$) and follows with a two solvent phase reduction to synthesize gold-thiolate nanoclusters.[14] Several modifications to the Brust–Schiffrin methods (i.e. changing the solvent, changing from two-phase to one-phase reactions) were then studied to refine the reaction process.[15,16] Recently, a mixture of diglyme (dg) and tetrahydrofuran (THF) solvents was applied to the gold-thiolate nanocluster self-assembly process, and diglyme can be observed as a ligand in the final generated product.[17–20] Diglyme was found to yield a gold-thiolate nanocluster dimer as well, which indicates that diglyme can mediate the gold nanoparticle assembly process.[18] Moreover, a $Au_{20}(SR)_{15}$-diglyme system was also found experimentally in which diglyme mediates dimerization of two nanoclusters to yield a photoluminescent cluster with a very high quantum yield.[21] Therefore, it is very important to investigate the interaction between diglyme and gold clusters which will help unravel the photoluminescent mechanism in these systems in the future.

With the growth of experimental research on ligand-protected gold nanoparticle synthesis,[14–16,22–25] the mechanisms involved in this process have also been investigated using quantum chemistry calculations.[26–30] A plausible reaction pathway from Au(III) chloride to Au(I) thiolate via the addition of thiols was first proposed by Barngrover and Aikens using the density functional theory (DFT) method in 2011, and the involved reaction pathways were demonstrated to be thermodynamically favorable.[26] Later, solvent effects and R group effects on the Au(III) to Au(I) reaction were examined theoretically.[27] The DFT method was also applied to study the Au nanoparticle growth pathway starting from gold halide complexes.[28] However, the previous discussions of the reaction mechanism were mainly focused on the original Brust–Schiffrin method. For the modified Brust–Schiffrin method that has diglyme as a solvent, the question arises: how does diglyme play a role in the gold nanocluster synthesis process?

In this work, we computationally model reasonable reaction pathways to generate Au(I)-containing species from the starting Au(III) complex. ^1H NMR spectra are calculated to examine the proton environment of the gold-diglyme system. The interactions between diglyme and gold-

containing species are discussed using chemical bonding theory. In this way, a plausible mechanism for the diglyme-assisted Brust–Schiffrin synthesis can be proposed.

Computational Details

All calculations were performed with the Amsterdam Modeling Suite (AMS) 2021.102 software.[31] Geometry optimizations were performed at the BP86/TZP level of theory with a frozen core approximation (1s for C, 1s for O, 2p for S, 2p for Cl, 4f for Au), where BP86[32,33] is a generalized gradient approximation (GGA) exchange-correlation functional and TZP stands for the triple-zeta polarized basis set. Scalar relativistic effects were included by using the Zero Order Regular Approximation (ZORA).[34,35] Grimme3 parameters were added to correct for the dispersion interaction.[36,37] Solvent effects were taken into consideration using the Conductor-like Screening Model (COSMO).[38–40] All reaction pathways were modeled in diethyl ether solvent, which is similar in dielectric constant and functionality to the diglyme and tetrahydrofuran (THF) solvents used experimentally.

Because ^{1}H NMR spectra are sensitive to the atomic environment, NMR is a powerful experimental tool to characterize geometric structure. In our current work, ^{1}H NMR spectra for three featured molecular systems were calculated with respect to TMS (tetramethylsilane), because it is the standard reference for NMR spectra, both experimentally and theoretically. To examine the chemical shifts, single-point energy calculations were performed without the frozen core approximation in the basis set. Then, ^{1}H NMR calculations were performed on all protons in the diglyme molecule. Finally, ETS-NOCV theory[41–44] (see details in SI) was applied to analyze the bonding between the gold moiety and the diglyme molecule and to compare the differences between the gold-thiolate system and the gold-chloride system.

Results and discussion

A. Proposed reaction pathways

Previous theoretical work has suggested two different pathways that lead to the reduction of Au(III) to Au(I).[26] Our proposed reaction mechanisms are initially based on this previous work; however, our current proposed reaction pathway includes the diglyme molecule throughout the

entire reaction pathway. The reaction mechanism consists of two main parts: 1. Au(III)-Au(III) linking in the presence of diglyme; 2. thiol addition reaction (including reduction of gold atoms).

1. Au(III)-Au(III) linking reactions:

For the proposed reaction mechanism, the first step is the binding between the gold-chloride complex and diglyme (dg). The reaction starts with a Au(III) complex (here we use $HAuCl_4$), which binds to the diglyme molecule, and the proton and one chloride from $HAuCl_4$ generate a HCl molecule and a $AuCl_3$ species that possesses a dative bond with diglyme (Reaction 1A, Figure 1A). Then, a second $HAuCl_4$ is added, which binds with the $(AuCl_3)$dg product to generate $(AuCl_3)_2$dg (Figure 1B) and release another HCl as well (Reaction 2A). The optimized structure of $(AuCl_3)_2$dg (Figure 1B) shows that two $AuCl_3$ moieties are bound to the diglyme, with two of the chlorides bridging the two gold atoms. The Au_2Cl_6 moiety is known to be the preferred structure for the $AuCl_3$ dimer.[45] The generated $(AuCl_3)_2$dg species can subsequently react with $HAuCl_4$ and generate a HCl and a $(AuCl_3)_3$dg species (Figure 1C, Reaction 3A). The reaction energies for 1A, 2A, and 3A are -0.90 eV, -0.46 eV, and -0.80 eV, respectively. These reaction energies indicate that the Au-Au linking reactions are thermodynamically favorable. Previous work has shown that transition states for similar reactions have barriers near 0.3 eV,[26] so we expect these reactions to have reasonable kinetics at room temperature, which is a common temperature for nanoparticle synthesis.[22,24] Due to the increased size of the present systems and the additional degrees of freedom with the addition of diglyme, transition state searches are not practical; however, the Au(III) and Au(I) species considered in this work are very close to those in Ref. 26. Due to the flexibility of the diglyme and PET ligands, it should be noted that the systems present experimentally may vary dynamically from the lowest energy isomers found in this work, but these calculations demonstrate that the reactions are thermodynamically feasible.

Reaction Scheme 1. Au(III)-Au(III) linking reactions

$$HAuCl_4 + dg \rightarrow (AuCl_3)dg + HCl \quad (1A)$$

$$(AuCl_3)dg + HAuCl_4 \rightarrow (AuCl_3)_2dg + HCl \quad (2A)$$

$$(AuCl_3)_2dg + HAuCl_4 \rightarrow (AuCl_3)_3dg + HCl \quad (3A)$$

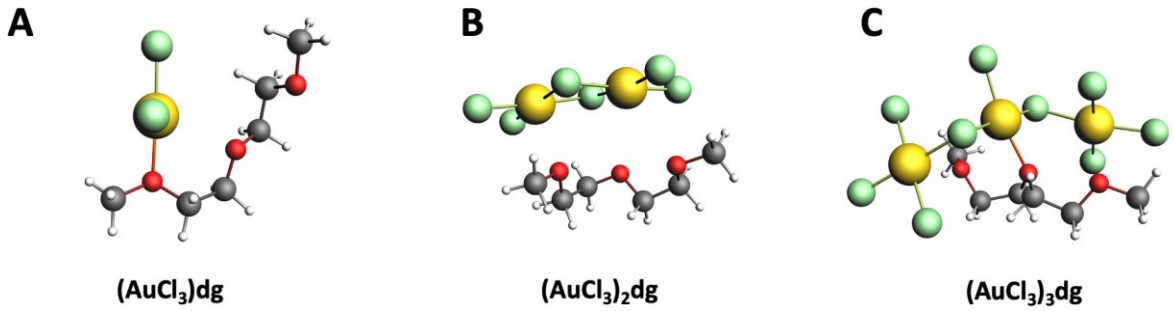

Figure 1. Three products in the Au-Au linking reactions. A. $(AuCl_3)dg$ B. $(AuCl_3)_2dg$ C. $(AuCl_3)_3dg$ Key: gold = gold, chlorine = green, carbon = grey, oxygen = red and hydrogen = white.

2. Thiol addition reactions:

For the thiol addition reactions, the $(AuCl_3)_2dg$ or $(AuCl_3)_3dg$ product can subsequently react with thiols to form a mixed Au(III)-Au(I) species. In this work, we focus on the species with two gold atoms as the simplest multi-atom species. 2-Phenylethanethiol (HPET, $HSCH_2CH_2Ph$) is used as the reactive thiol because it is the ligand used experimentally[18,19,21] in the formation of the known diglyme-containing nanoclusters. The added HPET reacts between the two Au atoms to bridge the two Au(III) species, and the proton on HPET reacts with one chloride to generate a $(AuCl_2)PET(AuCl_3)dg$ (Figure 2A) species and HCl (Reaction 1B), where PET is 2-phenylethanethiolate. The reaction energy for the first thiol addition is -0.97 eV, which is thermodynamically favorable. Then, the $(AuCl_2)PET(AuCl_3)dg$ species reacts with another thiol; the proton on the thiol reacts with a chloride to generate another HCl and product $(AuCl_2PET)_2dg$ (Figure 2B) with a reaction energy of -0.60 eV (Reaction 2B). Comparing between $(AuCl_3)_2dg$ and $(AuCl_2PET)_2dg$, we found that the gold chloride moieties tend to form a dimer and weakly bind to the diglyme molecule, whereas the mixed gold chloride-thiolate moieties tend to bind to the diglyme through coordinate covalent/dative bonding. The generated product $(AuCl_2PET)_2dg$ can continue to react with HPET to yield a disulfide $(PET)_2$ and the product $(AuCl_2)PET(AuCl)dg$ (Figure 2C) with a reaction energy of -0.79 eV (Reaction 3B). The resulting product, $(AuCl_2)PET(AuCl)dg$, is a mixed Au(III)-Au(I) species, in which one gold is in the +3 charge state and the other gold is in the +1 charge state. Formation of a disulfide is common in thiol-based reactions that reduce the oxidation state of gold.[15,26]

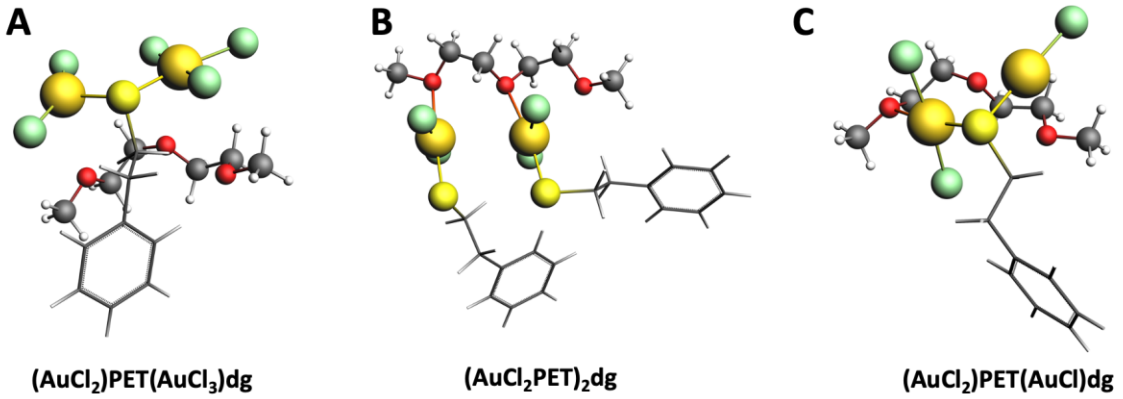

Figure 2. Three generated products for thiol addition reactions. The -$(CH_2)_2$-Ph (phenylethane) group is shown using a stick model. A. $(AuCl_2)PET(AuCl_3)dg$ B. $(AuCl_2PET)_2dg$ C. $(AuCl_2)PET(AuCl)dg$ Key: gold = gold, sulfur = light yellow, chlorine = green, carbon = grey, oxygen = red and hydrogen = white.

Reaction Scheme 2. Thiol addition reactions in the presence of diglyme

$(AuCl_3)_2dg + HPET \rightarrow (AuCl_2)PET(AuCl_3)dg + HCl$ (1B)

$(AuCl_2)PET(AuCl_3)dg + HPET \rightarrow (AuCl_2PET)_2dg + HCl$ (2B)

$(AuCl_2PET)_2dg + HPET \rightarrow (AuCl_2)PET(AuCl)dg + PET_2 + HCl$ (3B)

To compare the differences between the reaction energy with diglyme participants and without diglyme participants, the thiol addition reactions were modeled without the presence of diglyme molecule as well (Reactions 1B', 2B', and 3B'). The products for these reactions are shown in Figure 3A-C. Compared between the $(AuCl_2PET)_2dg$ (Figure 2B) and $(AuCl_2PET)_2$ (Figure 3B), we found the two $AuCl_2PET$ moieties will generate a dimer without the presence of the diglyme. The reaction energy results show that the reaction steps will be somewhat less energetically favorable when no diglyme is present in the molecular system (Table 1). These results indicate that diglyme can increase the exothermicity of the reaction for the thiol addition process.

Reaction Scheme 3. Thiol addition reactions without the presence of diglyme

$(AuCl_3)_2 + HPET \rightarrow (AuCl_2)PET(AuCl_3) + HCl$ (1B')

$(AuCl_2)PET(AuCl_3) + HPET \rightarrow (AuCl_2PET)_2 + HCl$ (2B')

$(AuCl_2PET)_2 + HPET \rightarrow (AuCl_2)PET(AuCl) + PET_2 + HCl$ (3B')

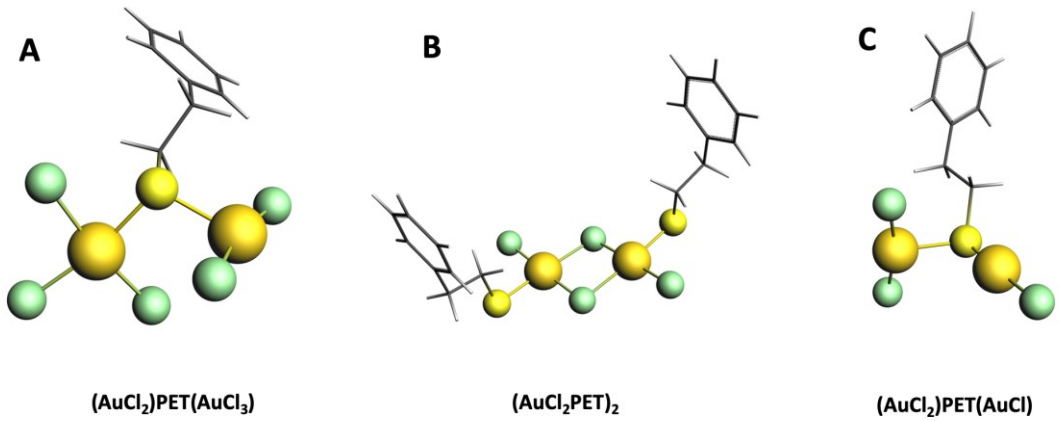

Figure 3. Three generated products for thiol addition reactions without diglyme; the -$(CH_2)_2$-Ph group is shown using a stick model. A. $(AuCl_2)PET(AuCl_3)$ B. $(AuCl_2PET)_2$ C. $(AuCl_2)PET(AuCl)$ Key: gold = gold, sulfur = light yellow and chlorine = green.

Table 1. Reaction energies for thiol addition steps (1B, 2B, 3B: diglyme present; 1B', 2B', 3B': no diglyme present).

Reaction index	Reaction energy (eV)	Reaction index	Reaction energy (eV)
1B	-0.97	**1B'**	-0.82
2B	-0.60	**2B'**	-0.26
3B	-0.79	**3B'**	-0.47

Next, the mixed Au(III)-Au(I) motif can continue to react with HPET to generate a motif that only contains Au(I) species. Two plausible pathways are considered as follows.

Reaction Scheme 4. Pathway 1

$(AuCl_2)PET(AuCl)dg + HPET \rightarrow (AuClPET)_2dg + HCl$ (1C)

$(AuClPET)_2dg + HPET \rightarrow (AuClPET)Au(PET)_2dg + HCl$ (2C)

$(AuClPET)Au(PET)_2dg + HPET \rightarrow (AuCl)PET(AuHPET)dg + PET_2$ (3C)

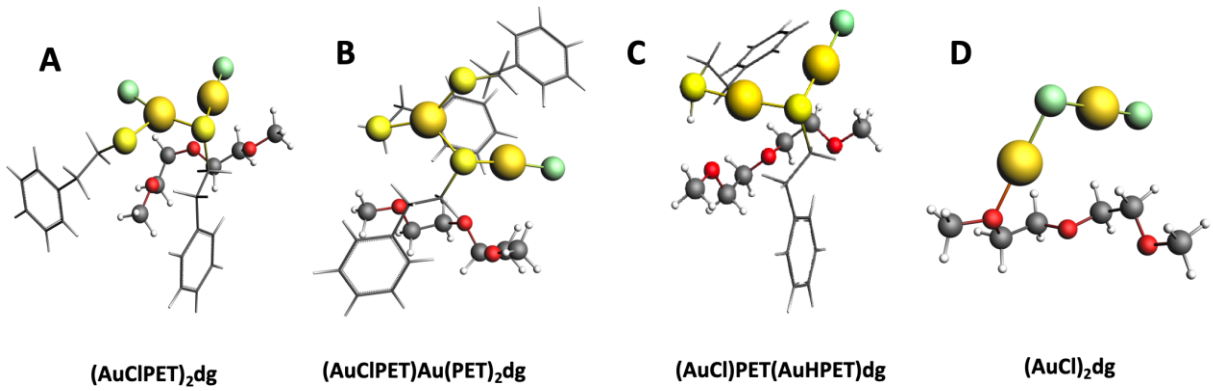

Figure 4. Four possible products formed in pathway 1 and pathway 2. The -$(CH_2)_2$-Ph group is shown using a stick model. A. $(AuClPET)_2dg$ B. $(AuClPET)Au(PET)_2dg$ C. (AuCl)PET(AuHPET)dg D. $(AuCl)_2dg$ Key: gold = gold, sulfur = light yellow, chlorine = green, carbon = grey, oxygen = red and hydrogen = white.

Pathway 1 One potential pathway is that the mixed Au(III)-Au(I) species $(AuCl_2)PET(AuCl)dg$ (Figure 2C) reacts with HPET. A chloride on Au(III) and the proton from the HPET generate a HCl, and then the PET binds to the gold to form $(AuClPET)_2dg$ (Figure 4A). This reaction energy is -0.01 eV (Reaction 1C). Then, $(AuClPET)_2dg$ can subsequently react with an additional HPET, and that HPET substitutes for a second chloride on the Au(III) atom to yield $(AuClPET)Au(PET)_2dg$ (Figure 4B) with a reaction energy of -0.62 eV (Reaction 2C). $(AuClPET)Au(PET)_2dg$ then reacts with a third HPET and generates a PET_2 molecule and (AuCl)PET(AuHPET)dg (Figure 4C, Reaction 3C). The reaction energy for this last step is -0.76 eV. The final product is a species that includes both Au(I)-thiolate and Au(I)-chloride motifs. Of note, the SR-Au-SR-Au-Cl moiety forms a V-shaped motif similar to the V-shaped staple motifs commonly found on the surface of gold nanoclusters.[4,46]

Reaction Scheme 5. Pathway 2

$$(AuCl_2)PET(AuCl)dg + HPET \rightarrow (AuCl)_2dg + PET_2 + HCl \quad (1D)$$

Pathway 2. Another pathway is that the Au(III)-Au(I)-mixed motif subsequently reacts with HPET to generate a disulfide (PET_2), HCl, and $(AuCl)_2dg$ (Figure 4D, Reaction 1D). Through this pathway, the mixed Au(III)-Au(I) motif can be transformed into a species with two Au(I)-chloride motifs. However, the calculated reaction energy is 1.13 eV, which indicates that the

endothermicity for the reaction is relatively high. Disulfides (and the corresponding gold reduction) are unlikely to be formed in this manner.

The reaction energies for the mechanisms discussed in this work are summarized in Table 2. (Reaction free energies with zero-point energy and entropic corrections are shown in the SI.) Comparing these two distinct pathways, pathway 1 generates both Au(I)-thiolate and Au(I)-chloride motifs, while pathway 2 generates a gold-chloride motif. Pathway 1 exhibits negative reaction energies for each step and exhibits an overall exothermic process, which indicates that it is a more thermodynamically favorable reaction pathway than pathway 2. Compared with previous calculations for systems without diglyme,[26] the synthetic pathway in the presence of the diglyme molecule shows more negative reaction energies for each step, which consequently indicates that the Au(III)-chloride motif can be reduced to a Au(I) motif with the assistance of diglyme in an energetically favorable pathway. We note that in the experiment, diglyme is present in great excess as a solvent; Le Chatelier's principle will likely aid in the formation of the diglyme-bound $AuCl_3$ species. In this work, we only considered the binding of a single diglyme to the gold systems, in part because only 1 or at most 2 diglyme species have ligated experimental nanoclusters,[17–21] although future work could consider the binding of additional diglyme molecules.

Table 2. Calculated reaction energies (eV) for each step in the investigated reaction pathways.

Reaction Index	Reaction energy (eV)
1A	-0.90
2A	-0.46
3A	-0.80
1B	-0.97
2B	-0.60
3B	-0.79
1C	-0.01
2C	-0.62
3C	-0.76
1D	1.13

B. Chemical shift analysis

^{1}H NMR calculations of the protons on the diglyme ligand were performed on three different species to examine how the protons of this ligand are affected by environment. Similar

calculations on the protons of the HPET moieties are discussed in the SI (Tables S1-S2, Figures S1-S2). The ^{1}H NMR spectra of the pure diglyme molecule was investigated previously and the theoretical chemical shifts lie in the range from 3.26 ppm to 3.98 ppm.[19] In ($AuCl_3$)dg (Figure 5A), $AuCl_3$ is a gold-chloride moiety with a +3 charge state for gold. The calculated ^{1}H NMR spectrum has chemical shifts that range from 3.35 ppm to 4.95 ppm (Table 3). Atom 13 has the highest chemical shift (δ = 4.95 ppm), and that proton is oriented close to a chloride on $AuCl_3$. Atom 10 shows a similar orientation to atom 13; its chemical shift is 4.60 ppm, which is the second-highest chemical shift. Atoms 21, 22, and 23 have the lowest chemical shifts; these three protons are located at the other terminal site of the diglyme molecule.

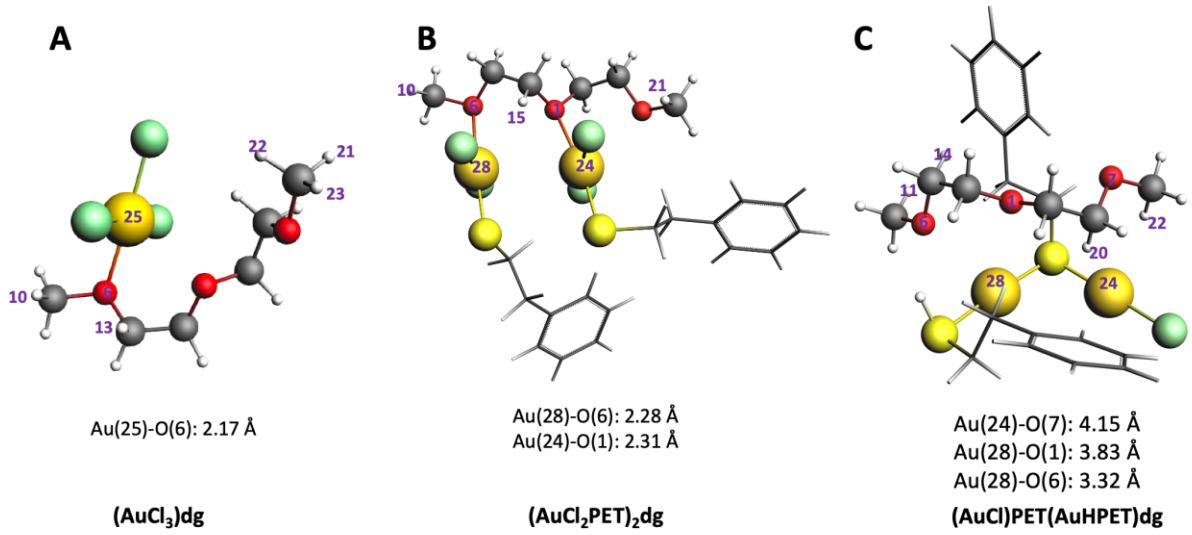

Figure 5. Optimized structures for A. $AuCl_3$dg, B. ($AuCl_2$PET)$_2$dg, and C. (AuCl)PET(AuHPET)dg. Selected geometric information and atom labels are also included. Full coordinates are given in the SI. Key: gold = gold, sulfur = light yellow, chlorine = green, carbon = grey, oxygen = red and hydrogen = white.

Table 3. Calculated NMR chemical shifts (ppm) for hydrogen atoms in diglyme ligand for $AuCl_3$dg, $(AuCl_2PET)_2$dg, and (AuCl)PET(AuHPET)dg.

$(AuCl_3)$dg		**$(AuCl_2PET)_2$dg**		**(AuCl)PET(AuHPET)dg**	
Atom Label	**δ (ppm)**	**Atom Label**	**δ (ppm)**	**Atom Label**	**δ (ppm)**
10	4.60	10	3.45	10	3.54
11	4.03	11	3.66	11	3.13
12	3.69	12	4.27	12	3.25
13	4.95	13	3.87	13	3.26
14	3.92	14	4.25	14	2.97
15	4.01	15	6.32	15	3.94
16	3.96	16	4.04	16	3.24
17	3.96	17	3.88	17	3.18
18	3.88	18	4.8	18	3.48
19	3.72	19	3.79	19	3.15
20	4.31	20	3.94	20	5.35
21	3.35	21	3.44	21	3.48
22	3.41	22	4.11	22	4.97
23	3.63	23	3.84	23	3.74

For $(AuCl_2PET)_2$dg (Figure 5B), two $AuCl_2PET$ motifs bind to two oxygen atoms of the diglyme molecule, and the two gold atoms are both in the +3 charge state. The ^{1}H NMR spectra have chemical shifts that range from 3.44 ppm to 6.32 ppm (Table 3). Atom 15 is located near two chlorides, and it has the highest chemical shift of 6.32 ppm. Atom 10 (δ = 3.45 ppm) and atom 21 (δ = 3.44 ppm) have the two lowest chemical shifts; these atoms are oriented away from the $AuCl_2PET$ moiety.

For the (AuCl)PET(AuHPET)dg system (Figure 5C), the two gold atoms are in the +1 charge state. The ^{1}H NMR spectra have chemical shifts ranging from 2.97 ppm to 5.35 ppm (Table 3). Atom 20, which is oriented towards the gold atom, has the highest chemical shift. Atom 22 has a very similar orientation to atom 20 and its calculated chemical shift is 4.97 ppm, which is the second-highest chemical shift. Atom 11 (δ = 3.13 ppm) and atom 14 (δ = 2.97 ppm) move upfield; both atoms are pointed towards the PET group.

Overall, by analyzing chemical shifts, the proton environment is observed to be strongly affected by the environment around diglyme. Protons that are oriented near gold and chloride will shift downfield, whereas protons that are pointed towards the PET group will move upfield. It was found experimentally in the diglyme-protected $Au_{20}(PET)_{15}dg_2$ system that some of the protons on diglyme move downfield significantly, and theoretical results suggest that these protons are located near the gold atoms in the nanocluster.[19]

C. Chemical bonding analysis

Because the interaction between diglyme and the Au-containing moieties is of significant interest in this work, the metal-oxygen bond in the molecular system is investigated using the ETS-NOCV chemical bonding theory. Geometric information and binding energies of the three systems featured in Figure 5 are examined to provide insights into the diglyme-gold interaction for various oxidation states of gold.

For the $(AuCl_3)$dg system, the Au-O bond distance is 2.17 Å (Figure 5A). For the $(AuCl_2PET)_2$dg system, two similar Au(III) moieties bind with diglyme, and the Au-O bond distances are calculated to be a little longer at 2.28 Å and 2.31 Å (Figure 5B). Compared with the mixed Au-thiolate and Au-chloride system $(AuCl_2PET)_2$dg, the pure Au-chloride $(AuCl_3)$dg system binds more tightly with the diglyme. The (AuCl)PET(AuHPET)dg system consists of a (AuCl)PET(AuHPET) motif and a diglyme ligand. In this system, the gold motif (which contains Au(I) species only) shows a weak interaction with the diglyme molecule, and all Au-O distances are above 3 Å (Figure 5C).

For $AuCl_3$dg, the binding energy between $AuCl_3$ and diglyme is -179.5 kJ/mol (Table 4). The strongest contribution to the charge transfer is from the oxygen atom on diglyme to chlorides on $AuCl_3$ (Figure 6) based on ETS-NOCV theory, and the corresponding orbital interaction energy is -126.4 kJ/mol. The interaction between diglyme and $AuCl_3$ leads to a total of 0.30 electrons (e) transferred from diglyme to the gold moiety (Table 4).

Table 4. Binding energy (kJ/mol) calculated using Eq. (1) between diglyme molecule and the gold moiety for three featured molecular systems. Charge analysis for three gold-diglyme systems using ETS-NOCV theory. The system is split into two fragments: diglyme and gold motif.

Molecular System	Binding Energy (kJ/mol)	Charge on Fragment 1 (dg)	Charge on Fragment 2 (gold motif)
$(AuCl_3)$dg	-179.5	0.30	-0.30
$(AuCl_2PET)_2$dg	-209.1	0.39	-0.39
(AuCl)PET(AuHPET)dg	-106.5	0.06	-0.06
$Au_{20}(SCH_3)_{15}dg^+$	-176.3	0.24	0.76

$$E_{binding} = E_{(system)} - (E_{(Au\ motif)} + E_{(diglyme)}) \quad (1)$$

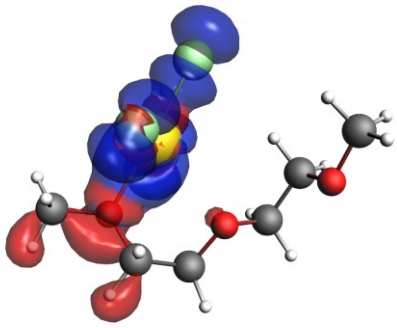

Figure 6. Dominant ETS-NOCV deformation density contribution for diglyme and $AuCl_3$ interaction. The charge flux is red to blue (isovalue = 0.001 au). Key: gold = gold, chlorine = green, carbon = grey, oxygen = red and hydrogen = white.

For $(AuCl_2PET)_2$dg, the binding energy between the two $AuCl_2PET$ moieties and diglyme is -209.1 kJ/mol (Table 4), which is higher compared with $AuCl_3$dg. Two dominant orbital interactions lead to the charge transfer, and the orbital interaction energies for these interactions are -77.9 kJ/mol and -77.3 kJ/mol, respectively (Figure 7). The first interaction is between the exterior oxygen and the exterior gold moiety. The second interaction is between the center oxygen and the center gold moiety. As a result, a total of 0.39 e was transferred from diglyme to the gold moieties (Table 4).

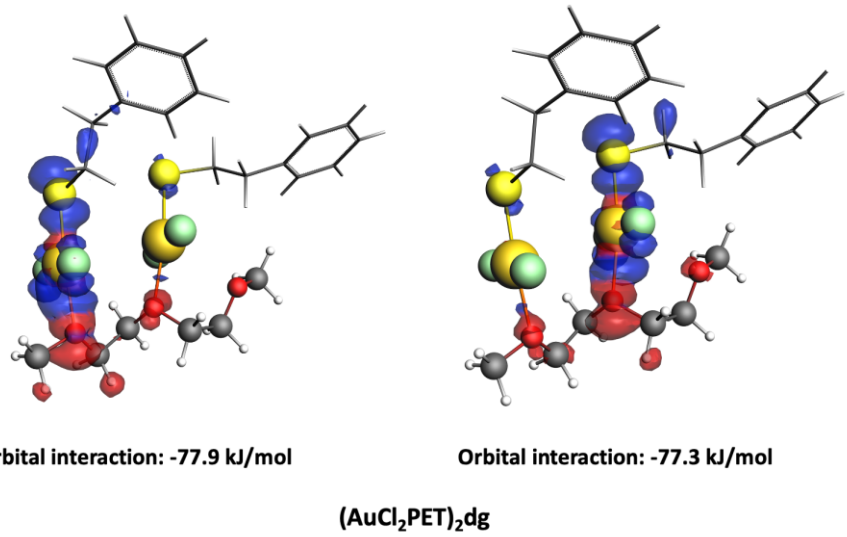

Figure 7. Dominant ETS-NOCV deformation density contributions for diglyme and $(AuCl_2PET)_2$ interaction. The charge flux is red to blue (isovalue = 0.001 au). Key: gold = gold, sulfur = light yellow, chlorine = green, carbon = grey, oxygen = red and hydrogen = white.

For (AuCl)PET(AuHPET)dg, the binding energy between the two fragments (diglyme and (AuCl)PET(AuHPET)) is -106.5 kJ/mol (Table 4), and only 0.06 e was transferred from diglyme to gold (Table 4). The dominant orbital interaction energy is -9.4 kJ/mol, which is relatively weak compared with the other two molecular systems (Figure 8). In this system, both Au atoms are in the +1 oxidation state and have two chloride or thiolate ligands, which causes the Au atoms to be less likely to accept electrons from the diglyme ligand.

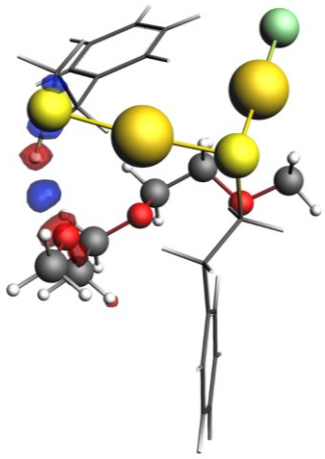

Orbital interaction: -9.4 kJ/mol

(AuCl)PET(AuHPET)dg

Figure 8. Dominant ETS-NOCV deformation density contribution for diglyme and (AuCl)PET(AuHPET) interaction. The charge flux is red to blue (isovalue = 0.001 au) Key: gold = gold, sulfur = light yellow, chlorine = green, carbon = grey, oxygen = red and hydrogen = white.

Since the diglyme has been found to have weak bonding with a gold nanocluster in experimental work,[18,19] the interaction between diglyme and $Au_{20}(SCH_3)_{15}^+$ was examined in the research as well. We started with the proposed $Au_{20}(SCH_3)_{15}dg^+$ computational model[19] and re-optimized the structure in diethyl ether solvent. The ETS-NOCV analysis shows a total of 0.24 electron (e) was transferred from diglyme to the gold nanocluster (Table 4). The dominant orbital interaction energy is -59.1 kJ/mol (Figure 9), and that orbital interaction energy is relatively weak compared with the interaction between the Au(III) species and diglyme.

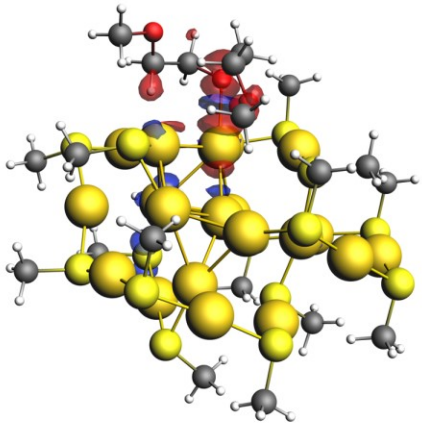

Figure 9. Dominant ETS-NOCV deformation density contribution for diglyme and $Au_{20}(SCH_3)_{15}^+$ interaction. The charge flux is red to blue (isovalue = 0.001 au). Key: gold = gold, sulfur = light yellow, carbon = grey, oxygen = red and hydrogen = white.

For $(AuCl_3)$dg and $(AuCl_2PET)_2$dg, the gold atoms are all in the +3 charge state, while in (AuCl)PET(AuHPET)dg and gold motifs in $Au_{20}(SCH_3)_{15}dg^+$, the gold atoms are in the +1 charge state. Both the binding energy results and the charge transfer analysis indicate that Au(III) species have relatively strong orbital interaction with diglyme compared with Au(I), while Au(I) has a more intense dispersion interaction with diglyme (Table 5).

Energy decomposition results (Table 5) for the gold motifs show that $(AuCl_2PET)_2$dg has the highest total interaction energy while (AuCl)PET(AuHPET)dg has the lowest total interaction energy. $(AuCl_2PET)_2$dg has the highest orbital interaction energy, which accounts for the highest charge transfer value. (AuCl)PET(AuHPET)dg system has the highest dispersion correction interaction energy, which is related to the dispersion-based bonding between two fragments.

For the $Au_{20}(SCH_3)_{15}dg^+$ system, the dispersion interaction energy (-182.6 kJ/mol) is higher than the orbital interaction energy (-150.8 kJ/mol). The total interaction energy is -178.8 kJ/mol, which is lower than the interaction energy (-209.5 kJ/mol) between diglyme and two $AuCl_2PET$ moieties. Since the gold atoms on the ligand-protected motifs are all in +1 charge states, the energy decomposition results demonstrate that the bonding between diglyme and Au(I) is weaker than the bonding between diglyme and Au(III).

Table 5. Bonding energy decomposition results for selected systems.

	$(AuCl_3)dg$	**$(AuCl_2PET)_2dg$**	**(AuCl)PET(AuHPET)dg**	**$Au_{20}(SCH_3)_{15}\ dg^+$**
Pauli Repulsion Energy (kJ/mol)	399.3	566.5	181.4	397.2
Electrostatic Interaction Energy (kJ/mol)	-340.3	-465.0	-130.3	-262.6
Orbital Interaction Energy (kJ/mol)	-179.5	-219.5	-62.2	-150.8
Dispersion Interaction Energy (kJ/mol)	-61.3	-107.0	-130.1	-182.6
Solvation Energy (kJ/mol)	2.2	15.4	34.4	19.9
Total Interaction Energy (kJ/mol)	-179.5	-209.5	-106.8	-178.8

Conclusion

A series of experimental studies have previously demonstrated that diglyme can mediate the synthesis of gold nanoclusters and assist with the self-assembly of gold nanoparticles. This work represents the first investigation of the intrinsic mechanism of diglyme-assisted synthesis. In the current research, by exploring plausible reaction pathways and calculating the reaction energy for each step, we propose a reasonable reaction mechanism for synthesizing gold-thiolate motifs in the presence of diglyme. The negative reaction energy in each step theoretically demonstrates that diglyme can assist the synthesis process of the gold nanocluster in an energetically favorable pathway.

By analyzing the NMR spectrum, we found that the diglyme ligand interaction on the gold motif can be characterized by examining the chemical shifts. Protons that are pointed towards chloride have chemical shifts that are shifted downfield, and protons that are pointed to the PET group will have low chemical shifts that may even lie upfield from the bare diglyme molecule. The NMR results in this work can be a good reference for the experimental research.

Finally, we applied the ETS-NOCV method to examine the chemical bonding of the featured system. We found that the Au(III)-chloride system can bind strongly with diglyme through dative bonding, while the Au(I)-thiolate moiety tends to form dispersion-based bonding with diglyme. The highest dispersion interaction energy was found in the $Au_{20}(SCH_3)_{15}\ dg^+$ system, and that demonstrates the weak bonding between diglyme and nanocluster. Comparing between the three featured systems, we can determine that the interaction between diglyme and gold motif becomes weaker when the oxidation state of gold is reduced from Au(III) to Au(I).

Supporting Information

Supporting information provides information on NMR spectra of protons in HPET groups, theoretical background of the ETS-NOCV theory, isomer energies, graphical version of chemical shift results, reaction free energies, and coordinates of selected isomers.

Acknowledgements

The work was supported by the U.S. National Science Foundation (CHE-1905048). A.L. and J.P. were supported by the NSF REU program (CHE-1852182). The computing for this work was performed on the Beocat Research Cluster at Kansas State University, which is in part funded by the NSF (Grant Nos. CHE-1726332, CNS-1006860, EPS-1006860, and EPS-0919443).

References

(1) Chen, H.; Liu, C.; Wang, M.; Zhang, C.; Luo, N.; Wang, Y.; Abroshan, H.; Li, G.; Wang, F. Visible Light Gold Nanocluster Photocatalyst: Selective Aerobic Oxidation of Amines to Imines. *ACS Catal.* **2017**, *7* (5), 3632–3638.

(2) Dreaden, E. C.; Alkilany, A. M.; Huang, X.; Murphy, C. J.; El-Sayed, M. A. The Golden Age: Gold Nanoparticles for Biomedicine. *Chem. Soc. Rev.* **2012**, *41* (7), 2740–2779.

(3) Saha, K.; Agasti, S. S.; Kim, C.; Li, X.; Rotello, V. M. Gold Nanoparticles in Chemical and Biological Sensing. *Chem. Rev.* **2012**, *112* (5), 2739–2779.

(4) Jin, R.; Zeng, C.; Zhou, M.; Chen, Y. Atomically Precise Colloidal Metal Nanoclusters and Nanoparticles: Fundamentals and Opportunities. *Chem. Rev.* **2016**, *116* (18), 10346–10413.

(5) Pei, Y.; Gao, Y.; Shao, N.; Zeng, X. C. Thiolate-Protected $Au_{20}(SR)_{16}$ Cluster: Prolate Au_8 Core with New $[Au_3(SR)_4]$ Staple Motif. *J. Am. Chem. Soc.* **2009**, *131* (38), 13619–13621.

(6) Zeng, C.; Liu, C.; Chen, Y.; Rosi, N. L.; Jin, R. Gold–Thiolate Ring as a Protecting Motif in the $Au_{20}(SR)_{16}$ Nanocluster and Implications. *J. Am. Chem. Soc.* **2014**, *136* (34), 11922–11925.

(7) Zhu, M.; Aikens, C. M.; Hollander, F. J.; Schatz, G. C.; Jin, R. Correlating the Crystal Structure of A Thiol-Protected Au_{25} Cluster and Optical Properties. *J. Am. Chem. Soc.* **2008**, *130* (18), 5883–5885.

(8) Akola, J.; Walter, M.; Whetten, R. L.; Häkkinen, H.; Grönbeck, H. On the Structure of Thiolate-Protected Au_{25}. *J. Am. Chem. Soc.* **2008**, *130* (12), 3756–3757.

(9) Heaven, M. W.; Dass, A.; White, P. S.; Holt, K. M.; Murray, R. W. Crystal Structure of the Gold Nanoparticle $[N(C_8H_{17})_4][Au_{25}(SCH_2CH_2Ph)_{18}]$. *J. Am. Chem. Soc.* **2008**, *130* (12), 3754–3755.

(10) Lopez-Acevedo, O.; Tsunoyama, H.; Tsukuda, T.; Häkkinen, H.; Aikens, C. M. Chirality and Electronic Structure of the Thiolate-Protected Au_{38} Nanocluster. *J. Am. Chem. Soc.* **2010**, *132* (23), 8210–8218.

(11) Qian, H.; Eckenhoff, W. T.; Zhu, Y.; Pintauer, T.; Jin, R. Total Structure Determination of Thiolate-Protected Au_{38} Nanoparticles. *J. Am. Chem. Soc.* **2010**, *132* (24), 8280–8281.

(12) Dass, A.; Nimmala, P. R.; Jupally, V. R.; Kothalawala, N. $Au_{103}(SR)_{45}$, $Au_{104}(SR)_{45}$, $Au_{104}(SR)_{46}$ and $Au_{105}(SR)_{46}$ Nanoclusters. *Nanoscale* **2013**, *5* (24), 12082.
(13) Pei, Y.; Wang, P.; Ma, Z.; Xiong, L. Growth-Rule-Guided Structural Exploration of Thiolate-Protected Gold Nanoclusters. *Acc. Chem. Res.* **2019**, *52* (1), 23–33.
(14) Brust, M.; Walker, M.; Bethell, D.; Schiffrin, D. J.; Whyman, R. Synthesis of Thiol-Derivatised Gold Nanoparticles in a Two-Phase Liquid–Liquid System. *J. Chem. Soc., Chem. Commun.* **1994**, *0* (7), 801–802.
(15) Goulet, P. J. G.; Lennox, R. B. New Insights into Brust−Schiffrin Metal Nanoparticle Synthesis. *J. Am. Chem. Soc.* **2010**, *132* (28), 9582–9584.
(16) Shaltiel, L.; Shemesh, A.; Raviv, U.; Barenholz, Y.; Levi-Kalisman, Y. Synthesis and Characterization of Thiolate-Protected Gold Nanoparticles of Controlled Diameter. *J. Phys. Chem. C* **2019**, *123* (46), 28486–28493.
(17) Armstrong, J.; Ackerson, C. J. The $Au_{25}(PMBA)_{17}$Diglyme Cluster. *Molecules* **2021**, *26* (9), 2562.
(18) Compel, W. S.; Wong, O. A.; Chen, X.; Yi, C.; Geiss, R.; Häkkinen, H.; Knappenberger, K. L.; Ackerson, C. J. Dynamic Diglyme-Mediated Self-Assembly of Gold Nanoclusters. *ACS Nano* **2015**, *9* (12), 11690–11698.
(19) Anderson, I. D.; Wang, Y.; Aikens, C. M.; Ackerson, C. J. An Ultrastable Thiolate/Diglyme Ligated Cluster: $Au_{20}(PET)_{15}(DG)_2$. *Nanoscale* **2022**, *14* (25), 9134–9141.
(20) Herbert, P. J.; Yi, C.; Compel, W. S.; Ackerson, C. J.; Knappenberger, K. L. Relaxation Dynamics of Electronically Coupled $Au_{20}(SC_8H_9)_{15}$-*n*-Glyme-$Au_{20}(SC_8H_9)_{15}$ Monolayer-Protected Cluster Dimers. *J. Phys. Chem. C* **2018**, *122* (33), 19251–19258.
(21) Herbert, P. J.; Ackerson, C. J.; Knappenberger, K. L. Size-Scalable Near-Infrared Photoluminescence in Gold Monolayer Protected Clusters. *J. Phys. Chem. Lett.* **2021**, *12* (31), 7531–7536.
(22) Sokołowska, K.; Malola, S.; Lahtinen, M.; Saarnio, V.; Permi, P.; Koskinen, K.; Jalasvuori, M.; Häkkinen, H.; Lehtovaara, L.; Lahtinen, T. Towards Controlled Synthesis of Water-Soluble Gold Nanoclusters: Synthesis and Analysis. *J. Phys. Chem. C* **2019**, *123* (4), 2602–2612.
(23) Yao, Q.; Chen, T.; Yuan, X.; Xie, J. Toward Total Synthesis of Thiolate-Protected Metal Nanoclusters. *Acc. Chem. Res.* **2018**, *51* (6), 1338–1348.
(24) Chen, T.; Fung, V.; Yao, Q.; Luo, Z.; Jiang, D.; Xie, J. Synthesis of Water-Soluble $[Au_{25}(SR)_{18}]^-$ Using a Stoichiometric Amount of $NaBH_4$. *J. Am. Chem. Soc.* **2018**, *140* (36), 11370–11377.
(25) Qian, H.; Zhu, Y.; Jin, R. Size-Focusing Synthesis, Optical and Electrochemical Properties of Monodisperse $Au_{38}(SC_2H_4Ph)_{24}$ Nanoclusters. *ACS Nano* **2009**, *3* (11), 3795–3803.
(26) Barngrover, B. M.; Aikens, C. M. The Golden Pathway to Thiolate-Stabilized Nanoparticles: Following the Formation of Gold(I) Thiolate from Gold(III) Chloride. *J. Am. Chem. Soc.* **2012**, *134* (30), 12590–12595.
(27) Neidhart, S. M.; Barngrover, B. M.; Aikens, C. M. Theoretical Examination of Solvent and R Group Dependence in Gold Thiolate Nanoparticle Synthesis. *Phys. Chem. Chem. Phys.* **2015**, *17* (12), 7676–7680.
(28) Barngrover, B. M.; Manges, T. J.; Aikens, C. M. Prediction of Nonradical Au(0)-Containing Precursors in Nanoparticle Growth Processes. *J. Phys. Chem. A* **2015**, *119* (5), 889–895.

(29) Matus, M. F.; Malola, S.; Häkkinen, H. Ligand Ratio Plays a Critical Role in the Design of Optimal Multifunctional Gold Nanoclusters for Targeted Gastric Cancer Therapy. *ACS Nanosci. Au* **2021**, *1* (1), 47–60.
(30) Li, L.; Wang, P.; Pei, Y. Mechanism of Nucleation of Gold(I) Thiolate Oligomers into Gold–Thiolate Nanoclusters. *J. Phys. Chem. C* **2022**, *126* (13), 5980–5990.
(31) te Velde, G.; Bickelhaupt, F. M.; Baerends, E. J.; Fonseca Guerra, C.; van Gisbergen, S. J. A.; Snijders, J. G.; Ziegler, T. Chemistry with ADF. *J. Comput. Chem.* **2001**, *22* (9), 931–967.
(32) Perdew, J. P. Density-Functional Approximation for the Correlation Energy of the Inhomogeneous Electron Gas. *Phys. Rev. B* **1986**, *33* (12), 8822–8824.
(33) Becke, A. D. Density-Functional Exchange-Energy Approximation with Correct Asymptotic Behavior. *Phys. Rev. A* **1988**, *38* (6), 3098–3100.
(34) van Lenthe, E.; Ehlers, A.; Baerends, E.-J. Geometry Optimizations in the Zero Order Regular Approximation for Relativistic Effects. *J. Chem. Phys.* **1999**, *110* (18), 8943–8953.
(35) Lenthe, E. van; Baerends, E. J.; Snijders, J. G. Relativistic Regular Two-component Hamiltonians. *J. Chem. Phys.* **1993**, *99* (6), 4597–4610.
(36) Grimme, S.; Ehrlich, S.; Goerigk, L. Effect of the Damping Function in Dispersion Corrected Density Functional Theory. *J. Comput. Chem.* **2011**, *32* (7), 1456–1465.
(37) Grimme, S.; Antony, J.; Ehrlich, S.; Krieg, H. A Consistent and Accurate *Ab Initio* Parametrization of Density Functional Dispersion Correction (DFT-D) for the 94 Elements H-Pu. *J. Chem. Phys.* **2010**, *132* (15), 154104.
(38) Klamt, A.; Schüürmann, G. COSMO: A New Approach to Dielectric Screening in Solvents with Explicit Expressions for the Screening Energy and Its Gradient. *J. Chem. Soc., Perkin Trans. 2* **1993**, No. 5, 799–805.
(39) Klamt, A. Conductor-like Screening Model for Real Solvents: A New Approach to the Quantitative Calculation of Solvation Phenomena. *J. Phys. Chem.* **1995**, *99* (7), 2224–2235.
(40) Klamt, A.; Jonas, V. Treatment of the Outlying Charge in Continuum Solvation Models. *J. Chem. Phys.* **1996**, *105* (22), 9972–9981.
(41) Michalak, A.; DeKock, R. L.; Ziegler, T. Bond Multiplicity in Transition-Metal Complexes: Applications of Two-Electron Valence Indices. *J. Phys. Chem. A* **2008**, *112* (31), 7256–7263.
(42) Nalewajski, R. F.; Mrozek, J.; Michalak, A. Two-Electron Valence Indices from the Kohn-Sham Orbitals. *Int. J. Quant. Chem.* **1997**, *61* (3), 589–601.
(43) Mitoraj, M. P.; Michalak, A.; Ziegler, T. A Combined Charge and Energy Decomposition Scheme for Bond Analysis. *J. Chem. Theory Comput.* **2009**, *5* (4), 962–975.
(44) Mitoraj, M. P.; Michalak, A.; Ziegler, T. On the Nature of the Agostic Bond between Metal Centers and β-Hydrogen Atoms in Alkyl Complexes. An Analysis Based on the Extended Transition State Method and the Natural Orbitals for Chemical Valence Scheme (ETS-NOCV). *Organometallics* **2009**, *28* (13), 3727–3733.
(45) Hargittai, M.; Schulz, A.; Réffy, B.; Kolonits, M. Molecular Structure, Bonding, and Jahn−Teller Effect in Gold Chlorides: Quantum Chemical Study of $AuCl_3$, Au_2Cl_6, $AuCl_4^-$, AuCl, and Au_2Cl_2 and Electron Diffraction Study of Au_2Cl_6. *J. Am. Chem. Soc.* **2001**, *123* (7), 1449–1458.
(46) Wan, X.-K.; Tang, Q.; Yuan, S.-F.; Jiang, D.; Wang, Q.-M. Au_{19} Nanocluster Featuring a V-Shaped Alkynyl–Gold Motif. *J. Am. Chem. Soc.* **2015**, *137* (2), 652–655.

TOC

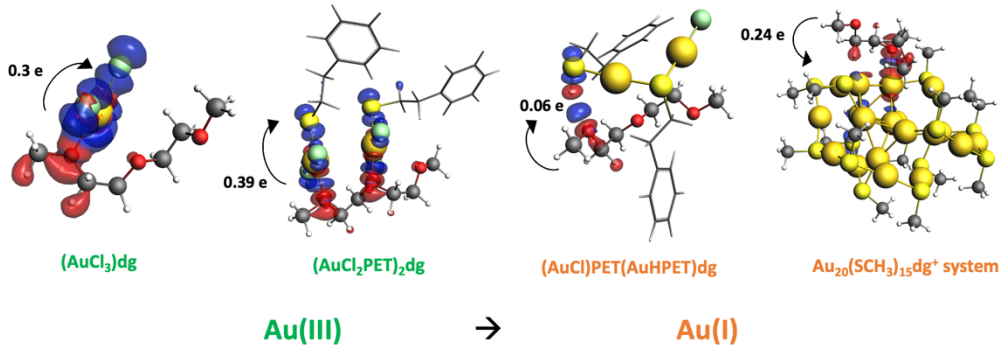
0.3 e
0.39 e
0.06 e
0.24 e
(AuCl3)dg
(AuCl2PET)2dg
(AuCl)PET(AuHPET)dg
Au20(SCH3)15dg+ system
Au(III)
Au(I)